Solute interface segregation measurement: Cross comparison between four different analytical method

Chih-Ying Hsu, J. Stodolna, P. Todeschini, F. Delabrouille, Vincent Barnier, Bertrand Radiguet, Frédéric Christien

Solute Interface Segregation Measurement: Cross Comparison between Four Different Analytical Methods

C.-Y. Hsu[1,2], J. Stodolna[1], P. Todeschini[1], F. Delabrouille[1], V. Barnier[2], B. Radiguet[3], F. Christien[2*]

1: EDF R&D, MMC Department, F-77250 Ecuelles, France

2: Mines Saint-Etienne, Univ Lyon, CMRS, UMR 5307 LGF, Centre SMS, F-42023 Saint-Etienne, France

3: Normandie Université, UNIROUEN, INSA Rouen, CNRS, Groupe de Physique des Matériaux, 76000 Rouen, France

Keywords: Solute Interface Segregation; Grain Boundary; Quantification; STEM-EDX; XPS; Atom Probe Tomography.

Abstract

Phosphorus intergranular segregation is known to influence the fracture properties of steels by decreasing grain boundary cohesion and induce intergranular fracture. Different techniques such as Angle-Resolved X-ray Photoelectron Spectroscopy (AR-XPS), Wavelength Dispersive Spectroscopy (WDS), Energy Dispersive X-ray Spectroscopy coupled with Scanning Transmission Electron Microscope (STEM-EDX), and Atom Probe Tomography (APT) can be used to quantify intergranular segregation. Although many studies of this phenomenon were conducted over the last decades, there are rarely direct comparisons between different techniques and there is still a need of reliable and comparable quantification methods for grain boundary segregation. This study cross-compares four available techniques (AR-XPS, WDS, STEM-EDX, and APT) to quantify phosphorus interfacial segregation within the same grain of a sample. This was done by fabricating a Fe-P-Fe sandwich specimen with phosphorus segregated at the interface. Attention was paid to the way of expressing the results of the different techniques so that they can be compared with one another. The quantification results from the different techniques show reasonable agreement.

1. Introduction

In a general way, interfacial segregation describes the rearrangement of solute atoms locally at planar defects, such as grain boundaries, precipitate-matrix interfaces, and free surfaces. It is important to experimentally identify and quantify this phenomenon, since it can strongly affect the cohesive energy of the interface, and thus the material properties. For example, in the nuclear industry, it has been shown that phosphorus intergranular segregation influences the fracture properties of steels [1]–[6]. Developing analytical methods for accurate quantification of phosphorus grain boundary segregation is crucial for understanding, modelling and predicting aging of heavy components in the nuclear industry.

The most common technique for grain boundary segregation identification and quantification is Auger Electron Spectroscopy (AES) [1]. However, the limitation of AES is the need of intergranular fractured surfaces that can only be obtained when there is a minimum amount of embrittling elements segregated. Also, these analyzable grain boundaries are often limited to prior austenite grain boundaries in bainitic or martensitic steels. In cases where intergranular fracture of the specimen cannot be obtained, the analysis of the grain boundaries using AES is simply not possible. This has raised difficulty to conduct research on representative materials where the bulk phosphorus content is low.

Besides AES, X-ray Photoelectron Spectroscopy (XPS) could also in principle be used for the analysis of grain boundary segregation. Nevertheless, due to its poor lateral resolution (some tens to hundreds of µm), the local analysis of grain boundary facets on a fracture surface is practically impossible. On the other hand, Wavelength Dispersive X-ray Spectroscopy (WDS) can also be adapted for intergranular segregation quantification. WDS analyzes both the signals from surface segregation and bulk. When analyzing with different accelerating voltages and adapting the quantification procedure, it is possible to separate the contribution of the surface segregation from the bulk. It was demonstrated that this method has excellent quantitative ability and is not as sensitive to surface contamination as AES [7], [8].

Different from previously mentioned techniques, Atom probe Tomography (APT) provides another approach to analyze intergranular segregation. Thanks to the development of Focus Ion Beam (FIB), it has become possible to select particular grain boundaries for APT analysis. Akhatova et al. [9] have described the method of preparing a single grain boundary on APT tips, and the method linking the segregation quantification to grain boundary characteristics. Zhang et al. [10] further adapted the method on industrial grade alloys to quantify segregated elements. However, APT has limitations for the analysis of grain boundary segregation, including the limited grain boundary area analysed, the difficulty of specimen preparation and the risk of specimen failure during analysis. Energy Dispersive X-ray Spectroscopy (EDX) equipped on Scanning Transmission Electron Microscope (STEM) also allows selecting particular grain boundary to analyze. It also has the advantage of possibly having multiple grain boundaries per sample and that the sample can be re-analyzed multiple times. However, in contrast to APT, STEM-EDX cannot analyse certain elements like H or Li. There have been some studies [11]–[16] using STEM-EDX as a method to quantify intergranular segregation. However, the main debate arises from the beam-specimen interaction (electron distribution, beam broadening) during analysis and how this affects the quantification of the segregated elements [12], [17]. The quantification procedures usually require different assumptions so that the measured apparent concentration can be expressed as the real grain boundary concentration. These assumptions are often the beam/matter interaction volume after beam broadening and the grain boundary thickness that can vary from different studies and are sometimes not specified.

Among the different characterization techniques mentioned above, different works were done to compare intergranular segregation measurements. Allart et al. [18] worked on sulfur segregation in nickel using AES and WDS, showing a linear relationship between the two techniques. Some authors worked on comparisons between STEM-EDX and AES [12], [19]–[22] in different systems. Their results are often based on different hypotheses for STEM-EDX quantifications and different interpretations of the peak height

ratio for AES measurements so that direct comparison is complicated. Akhatova et al. [9] compared phosphorus intergranular segregation results in a Fe-P model alloy from APT and AES, and found similar results. Furthermore, in a previous study [23], the authors of this paper have worked on comparing STEM-EDX and APT quantification results on the same grain boundaries as those studied by Akhatova [9]. They show that the results agree within 15%. Weidow et al. [24] measured segregations in WC doped with V, Cr, Mn using STEM-EDX and APT. However, no direct comparison was provided. The different limitations of each technique mentioned above are common problems shared in those studies. Direct comparisons of intergranular segregation quantifications are rarely provided. This may be due to the limited access to quite specific instruments (like APT or AES after in-situ fracture), as well as the difficulty to replicate measurements on the same grain boundary to allow direct comparison: for example, AES analysis of grain boundaries needs to fracture the specimen, which makes it a destructive technique, so that it is practically impossible to compare AES with other methods of measurements on a unique grain boundary.

Results of "concentration of intergranular segregation" can be presented in different units such as fractions of a monolayer [25], coverage ratios, atomic percentages [26], [27], and surface concentrations (atoms/unit surface) [9], [10], [12]. Some of those units need assumptions. For example, to express the segregation measurement as a fraction of a monolayer, it is needed to define a number of atoms in a monolayer. This can be easily calculated assuming for example that a monolayer is a close packed plane of the crystal structure (for example, (110) in BCC metals). On the other hand, the concept of coverage ratio needs to assume a number of segregation sites per unit area in the interface. Finally, the determination of an atomic percentage requires the definition of a grain boundary thickness. Unfortunately, some of these assumptions are not always clearly defined in literature, making comparison of results from different sources practically impossible.

The objective of this work is to cross-compare quantifications of segregation on one single interface using four different analytical methods: AR-XPS (angle-resolved XPS), WDS, STEM-EDX, and APT. To achieve that,

a surface approach was used first: a phosphorus doped iron substrate covered with a fractional monolayer of surface-segregated phosphorus was analyzed using XPS and WDS. Then, the phosphorus segregated layer was covered with a 100 nm layer of iron deposition. This creates a Fe-P-Fe sandwich to mimic a P-segregated grain boundary. FIB specimens were then cut from that "grain boundary" in order to conduct STEM-EDX and APT analyses on the same segregation layer as that analyzed using XPS and WDS. Particular attention was paid to express the results from the different techniques in the same unit (surface concentration). For each technique, a confidence interval of the measurement was determined using statistics considerations.

2. Material and Methodology

The approach developed in this work is based on a Fe – P – Fe (iron-phosphorus-iron) sandwich specimen, where phosphorus is present at the interface as a fractional monolayer. The material used as a substrate here is a disk (8 mm diameter, 0.6 mm thick) cut from a model Fe – 0.0011 wt%P alloy fabricated in the laboratory. The phosphorus concentration was verified by X-ray fluorescence spectrometry and WDS. It should be mentioned that trace amounts of sulfur (< 3 wt ppm) are also present in the model alloy used. The disk was polished down to colloidal silica. To ensure comparable results, a grain large enough for all techniques was identified. This is a compromise between the different spatial resolutions of the different techniques. A large grain was chosen due to the XPS beam size (selected to be at 400 µm), and the analysed volumes of other techniques were all within this grain. Figure 1 shows an optical micrograph of the sample surface, where the grain boundaries are marked in black. A scratch on the sample surface (white line) locates the grain of interest. The different acquisition zones for each technique are indicated in different colors. It is to be noted that the TEM thin foils and APT chunk are out of scale in Figure 1.

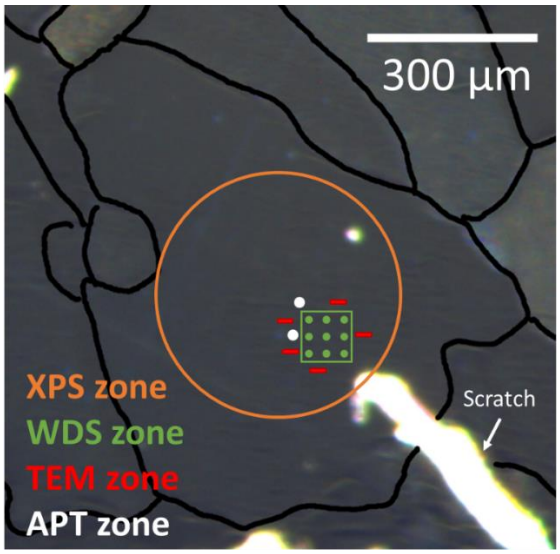

Figure 1: Optical micrograph of the polished Fe-P substrate. A large grain is identified and the different acquisition zones for each technique are marked. The grain boundaries are highlighted in black, the bright line is a scratch on the surface used for locating the grain of interest. XPS zone corresponds to the size of the primary X-ray beam, WDS zone is a 3x3 matrix of point analyses that covers 100 x 100 µm, TEM zones correspond to four FIB thin foils, APT zones are two chunks that result in five APT tips. The TEM thin foils and APT chunks are out of scale in this image.

The procedure of the sandwich specimen fabrication and the quantification by each technique are described in the following and illustrated in Figure 2.

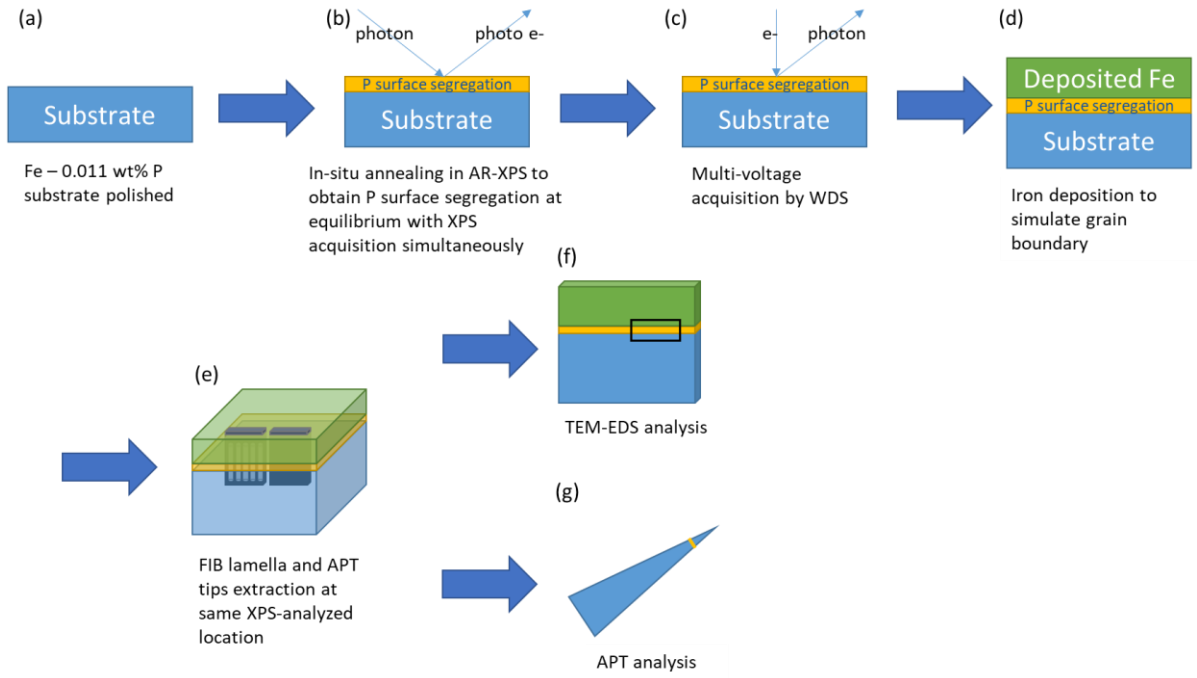

Figure 2: Schematic of the experimental procedure followed in this work.

The disc mounted on a resistive heater incorporated in the sample holder was introduced into the Ultra-High Vacuum analysis chamber (10^{-9} mBar) of a Thermo VG Thetaprobe spectrometer (Figure 2 (b)). XPS analysis was carried out with a focused monochromatic Al Kα source (hv =1486.68 eV, 400 µm spot size) and photoelectrons were collected using a concentric hemispherical analyzer operating in the constant ΔE mode and a 2D channel plate detector. The energy scale was calibrated with sputter-cleaned pure reference samples of Au, Ag and Cu such that $Au4f_{7/2}$, $Ag3d_{5/2}$, and $Cu3p_{3/2}$ were positioned at binding energies of respectively 83.98, 386.26 and 932.67 eV. After surface cleaning using Ar^+ ions, the disc was in-situ annealed at 500°C for 1 hour. The temperature was Proportional, Integral, Derivative (PID) controlled using a thermocouple welded to the surface of the analyzed specimen and fast acquisition of the P_{2p} peak was performed in snapshot mode using the 128 channels of the energy dispersive 2D detector axis in order to follow kinetics of phosphorus segregation. When equilibrium was reached, Angle-resolved XPS (AR-XPS) measurements were conducted thanks to the ability of the spectrometer to simultaneously

collect several photoelectron emission angles in acceptance range of 60° without tilting the sample. The photoelectrons were collected at six emission angles in the range of 25 to 75° with respect to the normal of the sample surface with 10° step. The acquisitions consisted of scanning the kinetic energy range of 1310 to 1450 eV with an analyser pass energy of 50 eV which gave energy resolution corresponding to a width of the $Ag3d_{5/2}$ peak measured on a sputter clean pure Ag sample of 0.55 eV. The XPS analyses were carried out in an acquisition zone (Figure 1) located in one single grain. It is to be noted that sulfur segregation was also observed during annealing, although the sulfur bulk content of the substrate material is below 3 ppm. However, the presence of segregated sulfur does not affect the procedure of phosphorus quantification. As segregation of P and S was observed at the surface, it was decided to quantify both elements in this study.

After XPS analysis, the disk was transferred to a Cameca SX-fiveFE Electron Micro Probe Analyzer chamber for WDS analysis (Figure 2 (c)). The specimen was carried at atmospheric pressure during transfer, so that the formation of a native surface oxide layer was inevitable. The problem of this oxide layer is treated later. However it was shown that WDS is not sensitive to nanometric oxide layers in contrast to XPS [7]. The multi-tension method proposed by Christien et al. [7] was performed with accelerating voltages of 5, 10, and 15 kV, and currents of 180, 250, and 233 nA in respect to each voltage. The electron beam was defocused at 10 µm. Analyses were conducted on a grid of 3x3 points (50 µm apart). The WDS acquisition locations are indicated in green in Figure 1. Two large pentaerythritol (PET) crystals with a 2d value of 8.75 Å were used. Considering the low segregated amount, the exact peak positions of P and S, expressed in $10^5 \sin(\theta)$, were determined on a standard material before acquisition at each accelerating voltage. The peak positions of phosphorus are 70407, 70407, 70404 and the peak positions of sulfur are 61381, 61395, 61364 at 5, 10 and 15 kV respectively. The peak intensity was obtained by measuring the counts at the peak maximum and then removing the background. The background positions, expressed in $10^5 \sin(\theta)$, were on the left (-750) and right (750) side of the peak positions. The acquisition was repeated twice at

the same positions to ensure that the surface contamination due to the electron beam has no effect. The standard materials used for this study are InP (In 78.76 wt% - P 21.24 wt%) and FeS_2 (Fe 46.55 wt% - S 53.45 wt%). The counting time corresponding to one single analysis was 2147 s at the peak position, and half the time at both the background positions.

Once the WDS analyses was completed, a thin layer of iron was deposited on top of the phosphorus and sulfur surface segregation layer at ambient temperature. Gatan Precision Etching and Coating System (PECS) using Ar^+ ions and a target of 99.99 wt% Fe (impurities are mainly Mn <800, C <200, P <200, S <150 wt ppm) was used. PECS was set to operate at 8 kV, the vacuum was optimized by flushing with argon and using a cold finger with liquid nitrogen. The pressure in the PECS chamber during deposition was about 10^{-3} Pa. At first, the sample was covered with a shutter so that the target can be cleaned. Then, the deposition was conducted in a sequence of six steps of five minutes, expecting around 100 nm of iron deposition. To avoid too much heating of the iron target, there was a 20 minute gap between each deposition step. As the temperature remains low during deposition, it is assumed that the deposition process does not induce phosphorus long-range diffusion. At the end, the sandwich specimen was obtained with the “surface” segregation layer between the substrate and the deposited iron, which was used to mimic grain boundary segregation.

Four TEM thin foils (Figure 2 (e)) were prepared using FEI Helios DualBeam FIB operating at 30 kV. The current used for final milling ranges from 920 nA to 28 nA. The FIB preparation was conducted so that the targeted interface is being aligned nearly edge-on (parallel to the TEM primary electron beam) right after FIB preparation (a few degrees off). Accurate edge-on condition is then obtained by slightly tilting the foil in the microscope. The final thicknesses of the thin foils were around 100 nm. The positions of thin foil extraction were random but all very close to the WDS acquisition zone and inside the XPS zone, indicated in red in Figure 2.

The STEM-EDX acquisitions (Figure 2 (f)) were performed in a FEI Tecnai OSIRIS TEM operating at 200 kV. The analytical system is based on the EDX FEI SuperX system using four windowless detectors. The setting of the beam was done to have about 30 kcps in total during EDX acquisitions, the beam condition was adjusted depending on the thin foil local thickness. The beam current under this criterion is around 0.5 nA and the beam size is about 1 nm. Elemental mapping was conducted using the hypermap function of Esprit v1.9 by Brukers was used. The mapping size was approximately 161 x 40 nm, giving a pixel size of 0.157 nm. The acquisition time was usually around 40 minutes for the entire map. The drift correction option in Esprit was used. The drift observed during the acquisitions was around 30 nm on average. These conditions were the same as in the authors' previous work in [23].

For APT analysis, two chunks were extracted within the same grain close to the acquisition zone of WDS (white areas in Figure 1) by conventional lift-out method, using a Zeiss XB540 dual beam. Five APT tips were prepared by annular milling from these chunks. In all cases, the interface was nearly perpendicular to the tip axis. Its position in the needle was checked after each milling step using transmission Kikuchi diffraction. When the distance between the interface and tip apex was smaller than 250 nm, the final milling step was performed using a Ga^+ ion energy of 2 keV to avoid contamination and implantation in the sample. This cleaning step was stopped when the interface was located at less than 50 nm from the tip apex. The interface composition was measured using a local-electrode atom probe (LEAP) 4000X HR from Cameca in voltage mode. The tips were cooled down to 69K. The pulse fraction was 20%, the pulse repetition rate was 200 kHz, and the detection rate was kept between 0.1 and 0.25%. The phosphorus segregated interface was analyzed successfully in three of the tips. In total, more than 1.5 million atoms were detected for each tip. The software IVAS 3.8 was used for reconstructing the analyzed APT tips. Since the Fe deposited layer and the substrate have different evaporation fields, the reconstruction was done considering a constant cone angle, estimated from scanning electron microscope images of the tips.

Typical parameters for ferritic steels were used for the reconstruction: image compression factor of 1.6 and field factor of 4.5. Further data treatment was performed using the GPM 3D software.

It is to be noted that all the analyses are carried out within the same initial grain (Figure 1). We assume that the surface of this grain can be considered a plane of given Miller index and that the segregation over the surface of that grain is reasonably homogeneous. Under this assumption, the analysed volume of the different techniques was chosen to be as close to each other as possible (see Figure 1), i.e. the WDS zone is within the XPS analyzed surface and the STEM-EDX FIB thin foils and APT chunks are beside and very close to the WDS analyzed zone.

3.1 Results & Discussions

3.1.1 Quantification by Angle resolved-XPS

Quantification of sub-monolayer of segregated P and S impurities in terms of surface concentration (atom/nm^2) was performed using the ratio of P_{2p} or S_{2p} photoelectron peak intensities to the one of Fe_{2p} peak obtained after removing a Tougaard inelastic background [28] from each spectrum acquired at the six different emission angles α: 25°, 35°, 45°, 55°, 65°, and 75°. Figure 3 shows examples of spectra obtained after background subtraction for a bulk sensitive configuration, i.e. using a photoemission angle close to the normal of the sample (α = 25°), and a surface sensitive one, i.e. using a grazing angle (α = 75°). P_{2p} and S_{2p} peaks are identified, which demonstrates the presence of phosphorus and sulfur surface segregation. In addition, increasing the emission angle increases the P_{2p} and S_{2p} peak intensity, relatively to Fe_{3p} peak intensity which is coherent with the presence of S and P at the extreme surface.

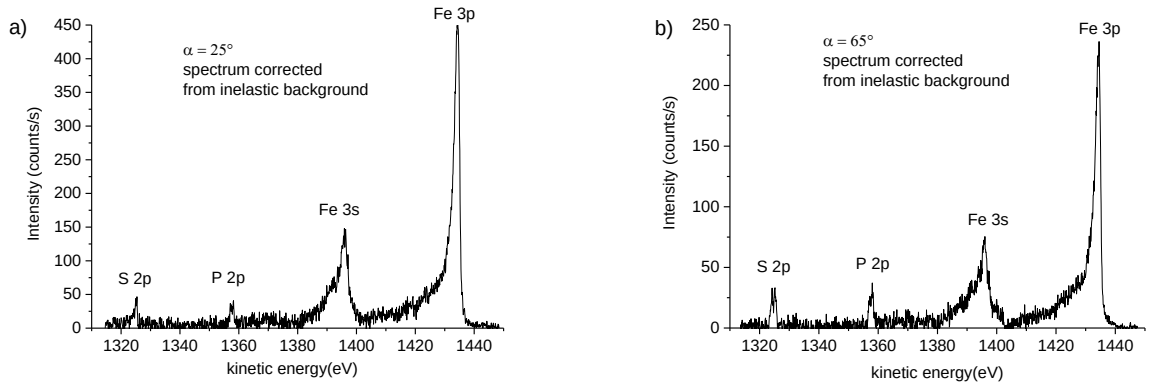

Figure 3: XPS spectra measured at emission angles of (a) 25° and (b) 65° of Fe sample annealed at 500°C for 1 hour in an ultrahigh vacuum. P and S surface segregation is evidenced.

The peak intensity ratio of P_{2p}/Fe_{3p} (or S_{2p}/Fe_{3p}) as demonstrated in appendix 1 has a linear relationship with the inverse of the cosine of the photoelectron emission angle α relative to the normal of the sample. This relationship is described by the following expressions for P_{2p} (the same type of expressions apply for S_{2p}):

$$\begin{aligned} &\frac{I_{P2p}}{I_{Fe3p}}.\frac{K_{Fe3p}}{K_{P2p}}.R=\frac{S_P}{\cos\alpha} \\ \text{with}\quad &K_{Fe3p}=\sigma_{Fe3p}W\left(\beta_{eff}^{Fe3p},\psi\right)Q_{Fe3p}^{(Fe)} \\ \text{with}\quad &K_{P2p}=\sigma_{P2p}W\left(\beta_{eff}^{P2p},\psi\right) \\ \text{and}\quad &R=N_{Fe}\lambda_{in}^{Fe}\left(E_{Fe3p}\right) \end{aligned} \qquad (1)$$

Where $I_{P_{2p}}$ and $I_{Fe_{3p}}$ are the P_{2p} and Fe_{3p} peak intensities obtained after Tougaard inelastic background subtraction, σ_x is the Scofield ionization cross-section of x core level (σ_{Fe3p} =1.669, σ_{P2p} =1.192, σ_{S2p} =1.67), $\lambda_{in}^{Fe}\left(E_{Fe3p}\right)$ is the inelastic mean free path of Fe_{3p} photo-electrons travelling through the Fe substrate ($\lambda_{in}^{Fe}\left(E_{Fe3p}\right)$ = 2.17 nm) which was calculated according to the TPP2M formalism [29]; S_P is the P surface concentration in atom/nm^2; N_{Fe} is the number of Fe atoms per unit volume in bulk iron (N_{Fe} =

85.5 atomatoms/nm^3) and S_{2p} is the surface concentration of P segregated atoms in atom/nm^2. The functions $Q_{Fe3p}^{(Fe)}$ and $W\left(\beta_{eff}^{Fe3p},\psi\right)$ are functions described in the appendix 1 taking respectively into account the elastic scattering effects in the substrate and the anisotropy of the differential photoelectric cross section depending on the angle ψ between the incident X-ray radiation and the photoemission and on the asymmetry parameter β_{eff}^{x} of the core level x .

Figure 4 shows the ratios I_{P2p}/I_{Fe3p} and I_{s2p}/I_{Fe3p} corrected from their respective factors $\frac{K_{Fe3p}}{K_{P2p}}.R$ and $\frac{K_{Fe3p}}{K_{S2p}}.R$ obtained at different emission angles as a function of $\frac{1}{\cos\alpha}$. Linear variations were obtained, in agreement with equation *(1)* and lead to phosphorus and sulfur surface concentrations of $S_{\mathrm{P}} = 3.38$ atom/nm^2 and $S_{\mathrm{S}} = 3.05$ atom/nm^2. The counting uncertainties on S_{P} and S_{S} were estimated from the standard error of the slopes extracted from the fit procedure. The results can be expressed as: $S_{\mathrm{P}} = 3.38 \pm 0.11$ atom/nm^2 and $S_{\mathrm{S}} = 3.05 \pm 0.08$ atom/nm^2.

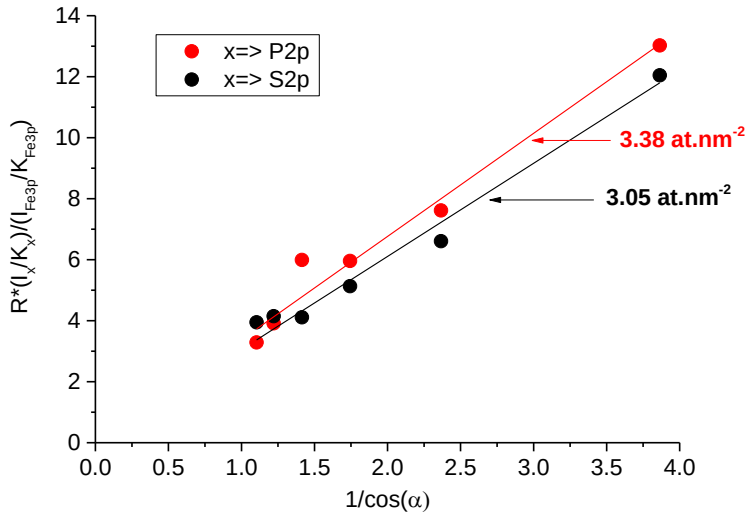

Figure 4: AR-XPS measurements. Peak intensity ratios I_{P2p}/I_{Fe3p} *and* I_{s2p}/I_{Fe3p} *corrected from their respective factors* $\frac{K_{Fe3p}}{K_{P2p}}.R$ *and* $\frac{K_{Fe3p}}{K_{S2p}}.R$ *described in equation (1) as a function of the inverse of the cosine of the photoelectron emission angle α relative to the normal of the sample. The measurements were conducted after one hour annealing treatment at 500°C in ultra-high vacuum.*

3.1.2 Quantification by multi-tension method using WDS

For WDS acquisitions, the multi-tension method proposed by Christien et al. [7] was applied. The relative intensity I/I_{Std} of phosphorus and sulfur are plotted in Figure 5 and Figure 6, respectively. I is the intensity (expressed in counts/s/nA) of the P Kα and S Kα line and I_{Std} is the intensity of the same line measured on the standard material. As expected, the relative intensity of both elements increases as the acceleration voltage decreases, indicating that the surface is enriched in both phosphorus and sulfur. Two series of measurements were conducted corresponding to square and triangle symbols in Figure 5 and Figure 6. These data points were fitted by a commercial software Stratagem™, following the same procedure as that presented in [7] in order to extract the phosphorus and sulfur surface concentrations. Stratagem™ is based on the model developed by Pouchou [30] for electron probe microanalysis of stratified specimens. Two stratified structures were defined in Stratagem™: the substrate is defined as iron containing 0.0011 wt%P. No sulfur was considered in the substrate as its content is below 3 wt ppm and has no effect at all on the calculations conducted using Stratagem™. For the first structure, a pure phosphorus surface layer was added on the substrate. For the second structure, a pure sulfur surface layer was added on the substrate. The mass thickness of the surface layer in both cases were adjusted so that the calculated curve can best fit the experimental points.

In the case of phosphorus segregation in Figure 5, the dashed line was calculated using Stratagem™ in the case when the sample surface is not enriched with phosphorus. In this case, the curve obtained depicts the contribution of bulk phosphorus only (0.0011 wt%). The continuous line shows the case where the

phosphorus surface segregation mass thickness was adjusted to 16.0 ng/cm^2, which is equal to 3.11 atom/nm^2. The same values of I/I_{Std} were obtained in the first and second measurements, which shows that there is no effect of surface contamination from the electron beam. As already mentioned earlier, the specimen was in contact with room atmosphere between AR-XPS and WDS analyses, so a native oxide layer covering the specimen surface is expected. STEM-EDX observation described later indeed showed a 3 nm thick oxide layer located on top of the segregation layer. An additional curve fit by Stratagem™ with a three-layer stratified structure was done, adding a layer of 3 nm Fe_2O_3 [31], [32] on top of the segregation layer. However, the phosphorus surface mass thickness extracted from the fit procedure was unchanged in this case (16.0 ng/cm^2), showing no influence from the native oxide layer on the quantification of the segregated element.

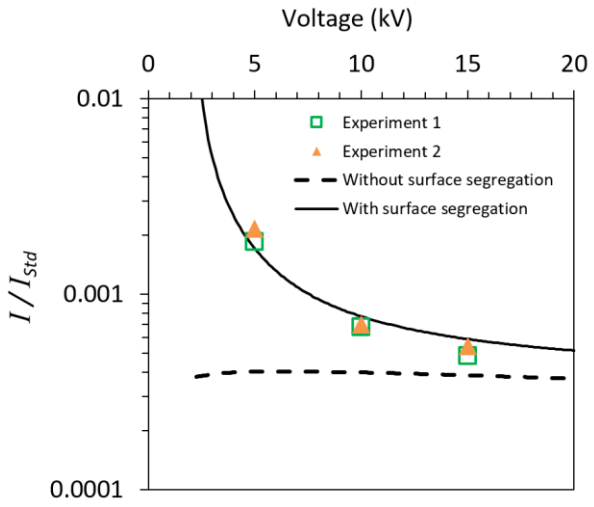

Figure 5: WDS measurements. Phosphorus relative intensities (log scale) versus accelerating voltage. Squares: first round acquisition. Triangles: second round acquisition. Lines: curves calculated using Stratagem™. Dashed line: only the phosphorus bulk content is considered (0.0011 wt% P). Continuous line: both phosphorus bulk content (0.0011 wt% P) and a phosphorus surface concentration of 16.0 ng/cm^2 = 3.11 atom/nm^2 are considered.

In the case of sulfur in Figure 6, the WDS measurements were more difficult than for phosphorus. The reason is that a 3rd order K peak of iron is located close to the S Kα peak. Although its intensity is very low,

it results in a significant overestimation of the background, resulting in underestimation of the S Kα peak intensity. This peak could not be completely discarded using the pulse height analyzer of the WDS spectrometer. In addition, attempts in shifting the background measurement position further from the S Kα peak also resulted in background overestimation. This spurious iron peak is located on the positive side of the sulfur peak. It should be mentioned that this problem does not exist at 5 kV as this voltage is not high enough to ionize the K level of iron, so that there is no iron spurious peak in this case. For the measurements conducted at 10 and 15 kV, the method of background measurement was changed between the first series of measurements (square symbols in Figure 6) and the second one (triangle symbols in Figure 6) in order to obtain the upper and lower limits of the S peak intensity. For the first dataset (squares), the conventional method was used, i.e. the background is measured on both sides of the sulfur peak (+750 and -750). In this case, the S peak intensity is underestimated. In the second dataset (triangles), the background is only measured at the negative side of the sulfur peak (-750), i.e. opposite to the spurious iron peak. However, because of the slope of the background, this results in an underestimation of the background, i.e. overestimation of the S peak intensity. The two datasets obtained at 10 and 15 kV give the upper and lower limits of the sulfur relative intensity. The sulfur surface concentration was adjusted in Stratagem^{TM} so that the calculated curve fits the measurements obtained at 5 kV. A sulfur concentration of 21 ng/cm^2 was obtained, which is equal to 3.94 atom/nm^2. It is to be noted that, as expected, the curve fit passes in between the two datasets at 10 and 15 kV.

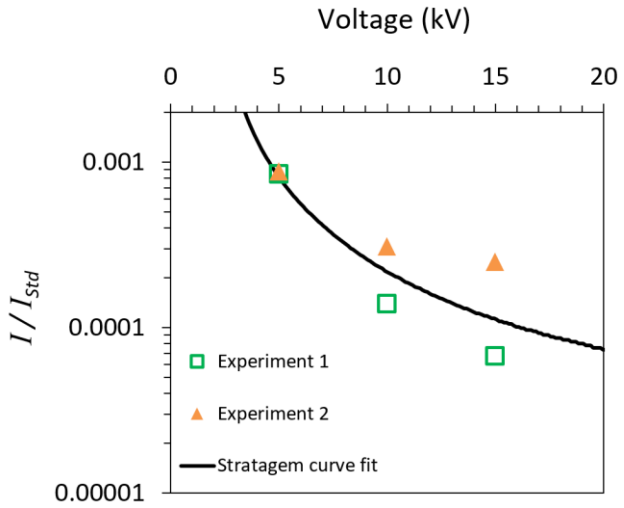

Figure 6: WDS measurements. Sulfur relative intensities (log scale) versus accelerating voltage. Square: first round acquisition. Triangle: second round acquisition. Line: curves calculated using Stratagem™ with a sulfur surface concentration of 21 ng/cm² = 3.94 atom/nm².

Christien et al. [7] conducted a detailed analysis of the statistical accuracy of surface segregation measurements using WDS. Following their approach (see Eq. 6 in [7]), the 68% confidence intervals of our WDS measurements of P and S segregation were determined at each accelerating voltage. It was found that the statistical accuracy achieved in this study is about 1%. This was permitted by the high beam current (250 nA) and very long counting times (38,646 s in total for each accelerating voltage). The final WDS results can be expressed as follows: $S_P = 3.11 \pm 0.03$ and $S_S = 3.94 \pm 0.04$ atom/nm².

3.1.3 Quantification by STEM-EDX

The STEM bright field image in Figure 7 shows a clear structure of the different layers: substrate / segregated layer / native oxide / deposited iron with different steps separated by oxide layers.

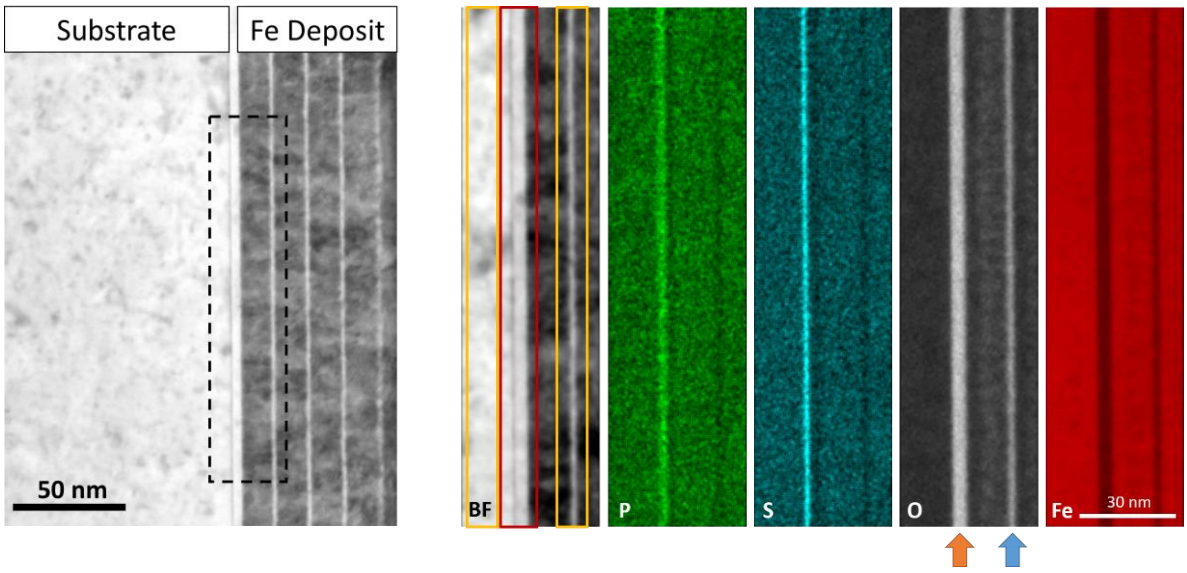

(a) (b)

Figure 7: STEM-EDX acquisition on the sandwich sample. (a) STEM BF image of one of the thin foils, the EDX acquisition zone is marked in black. (b) BF image and EDX element maps of Fe, P, S, and O.

Sharp interfaces can be seen, meaning that those interfaces are well aligned vertically, i.e. parallel to the electron beam. The substrate and the iron deposit were not aligned in zone axis for the mimic grain boundary to be aligned. Phosphorus and sulfur segregation are found at the substrate/oxide interface in Figure 7 (b), which is expected as the oxide formed after the segregation layer. The native oxide thickness is about 3 nm (orange arrow in Figure 7 (b)). In the iron deposition, there are different layers that correspond to the sequences during deposition. Oxide layers formed between each deposited layer due to the pause between each step. One of these oxide layers can be seen in Figure 7 (b) (blue arrow). The importance of keeping one of these oxide layers in the acquisition zone will be discussed later. Figure 8 shows line scans of the different elements across the different layers. Those line scans were obtained from vertical averaging of the EDX map. It confirms that phosphorus and sulfur segregation are located at the substrate/oxide interface. There are two oxygen peaks: the one on the left corresponds to the native oxide

covering the segregation layer, the second one is related to an intermediate oxide layer that formed between two steps of iron deposition.

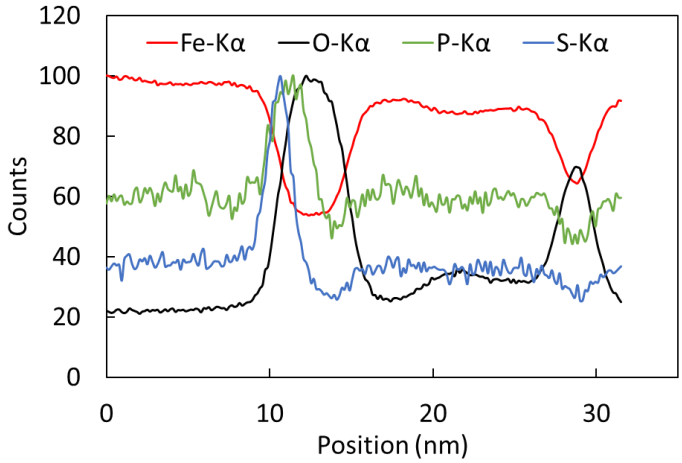

Figure 8: Line scans obtained from vertical averaging of the STEM-EDX mapping of Figure 7 (b).

In total 29 STEM-EDX acquisitions at different positions were performed on the four thin foils. For STEM-EDX acquisitions, a similar data treatment procedure as in the previous work by the authors [23] was applied. This procedure relies on three boxes extracted from the STEM-EDX maps. The central box contains the grain boundary (GB) to be analyzed. The two others are located on the left and on the right of the central box and that allows for the obtaining of a reference spectrum used for spectrum background removal. As shown in [23], background removal is critical to obtain accurate P and S peak intensities. Figure 7 shows an example of maps obtained from STEM-EDX. The three boxes selected are shown in red and yellow in Figure 7 (b). The central GB box contains the simulated grain boundary, as well as the native oxide. The left box is entirely located in the iron substrate and the right box is in the iron deposit. The right box was selected so that it contains an intermediate layer of oxide. This was done deliberately in order to include an oxide contribution to the reference spectrum background shape. Figure 9 (a) compares the GB spectrum (central box) and the reference spectrum (the two yellow boxes), where the X-ray intensity is

expressed in number of counts per second (cps), obtained for this particular acquisition. The reference spectrum $P_{Reference}$, expressed in counts per second (cps), is obtained from:

$$P_{Reference} = \frac{B_{sub} + \gamma\, B_{dep}}{t_{sub} + t_{dep}} \qquad (2)$$

where B_{sub} and B_{dep} are the "substrate" and "iron deposition" spectra (yellow boxes Figure 7 (b)), expressed in counts, γ is an adjustable parameter used to balance background contribution from "substrate" and "iron deposition" boxes ($\gamma = 1.2 - 1.5$) , t_{sub} and t_{dep} are the counting times corresponding to "substrate" and "iron deposition" boxes (i.e. number of pixels in the box times the counting time per pixel). An adjustable parameter γ was needed here to obtain identical background shapes for the GB and reference spectra. This is due to the contribution of oxides to the background shape: the γ parameter makes it possible to have the same oxide contribution in the two spectra. Figure 9 (a) and (b) shows the comparison between the GB spectrum and the reference one. The background shapes obtained are very similar, which allows correct background removal. A peak from Pt Mα and Zr Lα is found very close to P Kα. As detailed in [23], Pt comes from the FIB preparation and Zr from the EDX detector. However, the presence of these spurious peaks do not particularly complicate the P peak extraction. The Ag peaks are not identical on both spectra (silver is a contamination of the deposit). Again this does not affect the P and S peaks.

The net phosphorus Kα peak and net sulfur Kα peak were obtained by subtracting the reference spectrum from the GB one (Figure 9 (c)). Gaussian functions were fitted to the peaks to determine the phosphorus and sulfur peak intensities. The iron peak intensity was obtained in the same manner by fitting a Gaussian function to the iron Kα peak directly on the substrate spectrum (Figure 9 (d)).

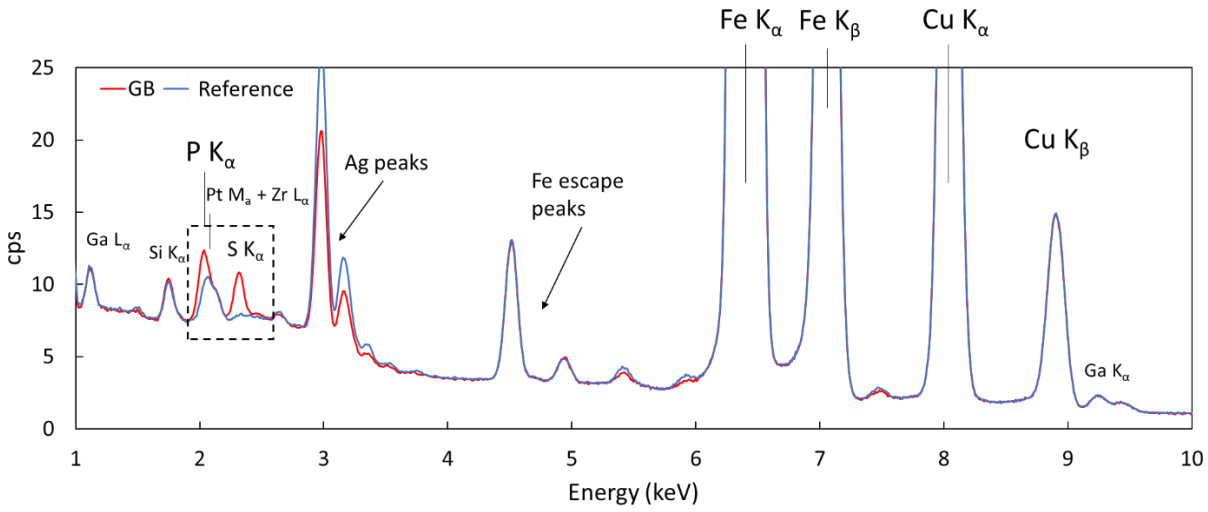

(a)

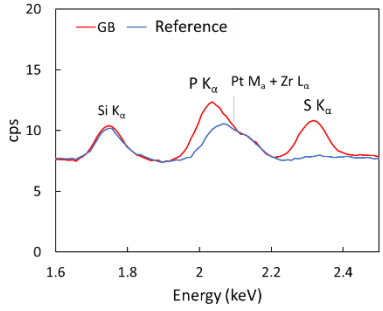

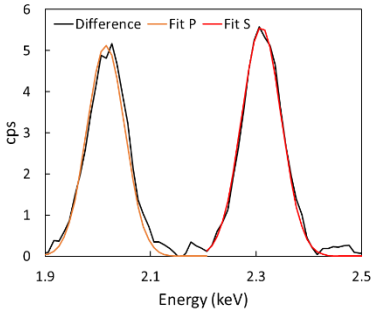

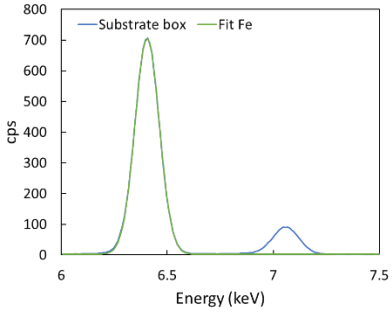

(b) (c) (d)

Figure 9: STEM-EDX data treatment: (a) superposed GB spectrum (corresponding to the red box in Figure 7 (b)) and reference spectrum (corresponding to two yellow boxes in Figure 7 (b)), (b) zoom in of (a) at the energy range close to P Kα and S Kα peaks, (c) P Kα and S Kα peaks after background subtraction (GB spectrum minus reference spectrum) fitted by a Gaussian function, (d) Fe Kα and Fe Kβ peaks from the substrate spectrum (corresponding to the left yellow box (b)) fitted by a Gaussian function.

The Cliff-Lorimer [33] method is used to quantify phosphorus and sulfur, the adapted formula is [23]:

$$C_i = \frac{k_{i/Fe} * ACF_{i/Fe} * \frac{I_i}{I_{Fe}}}{1 + \sum_i \left(k_{i/Fe} * ACF_{i/Fe} * \frac{I_i}{I_{Fe}} \right)} \quad (3)$$

where C_i is the concentration of element i (phosphorus, sulfur), $k_{i/Fe}$ is the k factor of element *i* in respect to iron, $ACF_{i/Fe}$ is the absorption correction factor of element *i* in respect to iron, $\frac{I_i}{I_{Fe}}$ is the intensity ratio

of the element *i* Kα peak and Fe Kα peak. The k factors used in this study are: $k_{P/Fe} = 0.790$ [23] and $k_{S/Fe} = 0.786$ [34]. ACF for each element are calculated based on the same method mentioned in [23]. The interface segregation can be expressed in atom/nm^2 using [12], [23]:

$$S_i = wN\frac{A_{Fe}}{A_i}C_i \qquad (4)$$

where S_i is the interface concentration of element *i* in atom/nm^2, N is the matrix density in nm^{-3} (85.5 nm^{-3} for iron), A_{Fe} and A_i are the atomic mass of iron and element *i*, respectively, *w* is the GB box width.

It should be mentioned that an adaptation from the method proposed by Hsu et al. [23] was done here. In [23], the iron peak intensity considered in the Cliff-Lorimer equation is that from the GB box. Instead here, the iron peak intensity from the *substrate box* is considered. This modification is to avoid the underestimation of iron peak intensity induced by the native oxide layer present in the GB box. Indeed, when the electron beam interacts with the oxide layer, the iron signal is lower than in pure iron (see Figure 8). So taking the iron peak intensity form the GB box would in turn result in overestimating the P and S concentration when using the Cliff-Lorimer equation (Eq. (3)). It is to be mentioned that this adaptation is valid only because the amounts of P and S measured in the GB box are low (on the order of 0.5 wt%).

Among 29 acquisitions in four thin foils, the average of phosphorus and sulfur segregation obtained are $S_P = 4.22 \pm 0.01$ atom/nm^2 and $S_S = 3.86 \pm 0.01$ atom/nm^2. The results are slightly higher than what was measured by XPS and WDS, but remain reasonably close. The uncertainties given here were obtained using Eq. (5) based on counting statistics [23]:

$$\frac{\Delta S_P}{S_P} \cong \frac{\sqrt{N_P^T}}{N_P} \qquad (5)$$

where S_P is the phosphorus grain boundary concentration, N_P^T is the total number of counts in the P energy window (1.9 – 2.2 keV) summed over the 29 acquisitions, and N_P is the number of counts in the P peak summed over the 29 acquisitions. The same equation also applies for sulfur.

3.1.4 Quantification by 3D reconstruction of APT

Figure 10 shows the 3D reconstruction of one of the APT tips. In the first reconstruction, only ions of P^+ and molecular ions PO^{2+} are represented, revealing clearly the phosphorus-enriched interface. In the second reconstruction, ions and molecular ions of oxygen are presented, showing one oxide layer in the iron deposit and another layer at the interface. It has to be mentioned that S segregation cannot be quantified with APT in this system since the interface is highly enriched in oxygen and the main S isotope has a mass of 32 Da so that S^+ is overlapped with O_2^+ and S^{++} is overlapped with O^+.

Figure 11 shows the cumulative concentration profiles of phosphorus, oxygen and silver, the latest being an impurity in the deposit. The phosphorus interface concentration was obtained directly from the cumulative concentration profile as shown in Figure 11. In the case of silver, there is no enrichment at the interface. The cumulative profile of silver (blue line in Figure 11) increases in the deposit and then remains nearly horizontal starting from the interface. Silver was chosen to represent the non-segregated agent due to its nature of pure contamination in the deposit. In the case of phosphorus, there is an enrichment at the interface. The slope of the phosphorus profile (orange line in Figure 11) increases between the iron deposit and the substrate. Similarly, the oxygen cumulative profile (green line in Figure 11) shows the two oxide layers with the changes in slope.

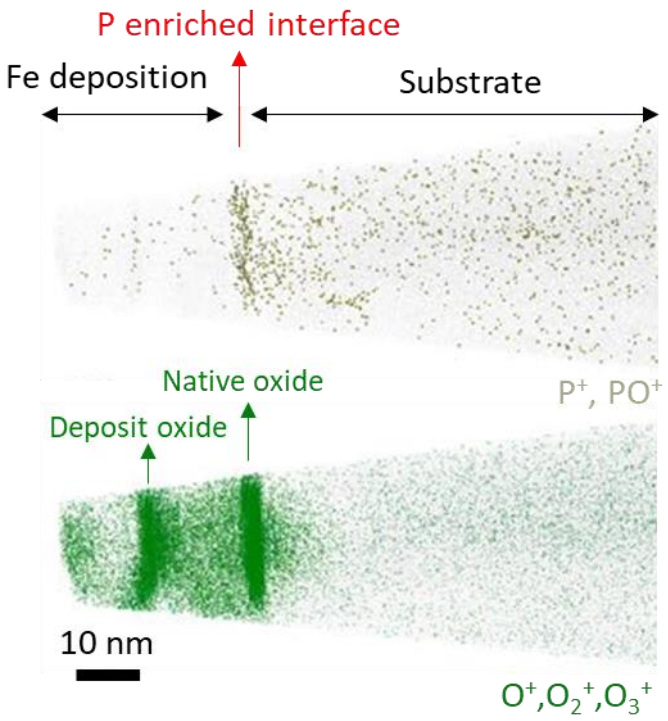

Figure 10: 3D reconstruction of one of the APT tips where phosphorus segregation is evident at the interface and oxide layers in the iron deposit and at the interface.

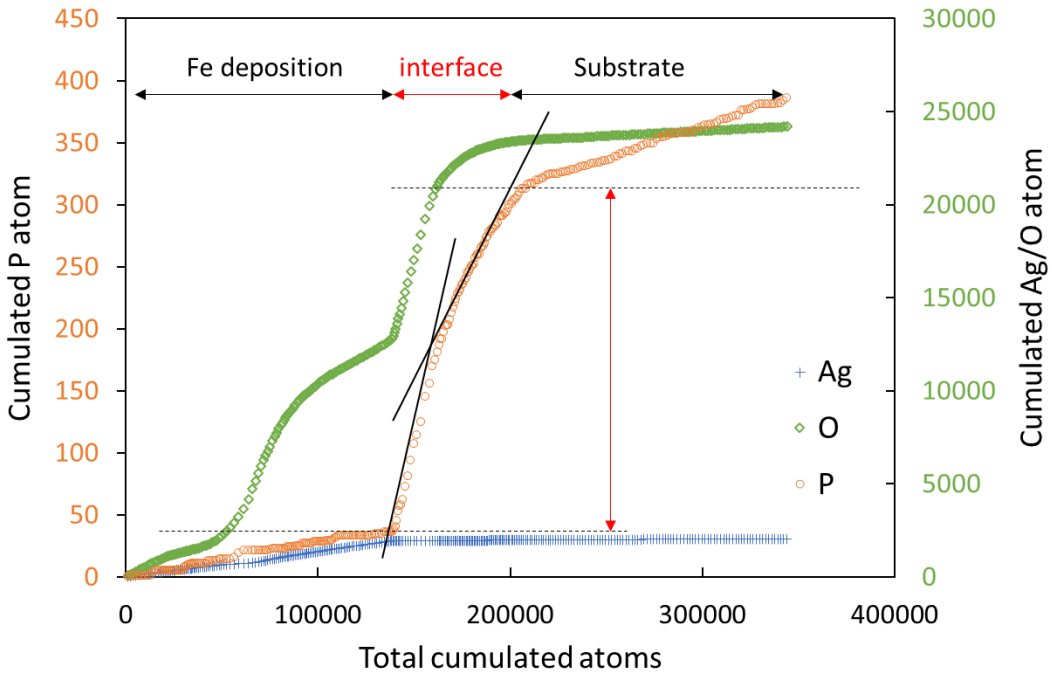

Figure 11: Cumulative concentration profiles of phosphorus, oxygen, and silver atoms determined from a cylindrical region perpendicular to the interface.

The interface enrichment of phosphorus is considered as the “interface concentration” instead of the “Gibb’s excess” as defined in [9]. The quantification (red double arrow) was directly defined by the difference between the two horizontal dashed lines in Figure 11 corresponding to the positions where the iron deposit ends and where the substrate starts. Questions have been raised about the slope changes at the interface (black continuous lines in Figure 11), which was not observed in actual grain boundary segregations [9]. A possible explanation is that the iron deposit and iron substrate, although close in composition, have different microstructures, the deposit being nanocrystalline and highly defective, so that the evaporation field during analysis changed at the interface. This assumption is supported by the voltage increase when entering into the substrate. This may have affected how the segregated phosphorus evaporated and contributed to delayed evaporation of phosphorous. Figure 12 shows the phosphorus concentration profile through the interface, from deposit to substrate. This profile is from the same tip as in Figure 11. Instead of having a sharp and symmetric peak, the phosphorus profile has a tail that covers about 15 nm in the substrate side. P diffusion from the substrate to the interface and equilibrium segregation at interface cannot result in such profile. Thus, P atoms contributing to the apparent tail on the profile likely come from the interfacial segregation and their field evaporation is delayed. This conclusion justifies including these P atoms in interfacial segregation measurement.

The phosphorus segregation measurements from the three tips gave an average of 4.6 atom/nm^2. No analysis of the counting uncertainty was conducted on the APT data in this study.

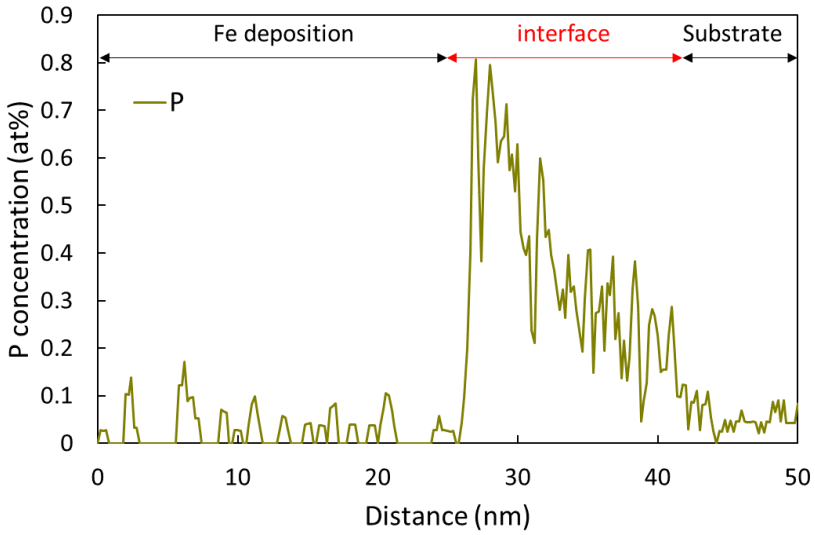

Figure 12: Phosphorus concentration profile in at% from the APT analysis. The data is from the same tip as in Figure 11.

3.1.5. Summary of the quantification results

At last, TTable 1 presents a summary of the phosphorus and sulphur segregation quantification results of each technique. The standard deviation between the different methods is of ± 0.7 atom/nm² for P and 0.5 atom/nm² for S. So the values obtained are in reasonable agreement with each other, considering that all the methods used are very different in nature. However, it can be observed that the confidence intervals of the different measurements do not overlap. We remind that those confidence intervals indicate the statistical accuracy of the results, i.e. they are entirely related to the counting statistics of each method. The fact the confidence intervals of the different measurements do not overlap means that the deviation between the different techniques is not only related to counting statistics. In other words, they are other biases affecting the measurements.

The first hypothesis to explain the differences between the results obtained from the different techniques is related to the homogeneity of the segregation concentration within the area investigated. We remind

here that, although all the measurements were conducted within the same grain (Figure 1), the location of the analysis could not be exactly the same for the different techniques. In case the segregation concentration would not be homogeneous within the area investigated, this could lead to different quantifications among the different methods. So it is critical to assess the homogeneity of the segregation concentration within the grain investigated (Figure 1). To do this, we will rely on the four different STEM-EDX thin foil studied. Among the four methods used, STEM-EDX is actually the one having the best statistical accuracy. It is then the best method to evidence possible local differences in the segregation concentration. Table 2 shows the STEM-EDX segregation quantifications obtained for phosphorus on the four thin foils extracted at different locations, as shown in Figure 1. In Table 2, the uncertainties were obtained using Eq. (5) based on counting statistics [23]. The difference in quantification between different thin foils can be significant (up to about one atom/nm²). On the other hand, the counting uncertainty obtained on each foil is very limited (0.02 atom/nm² for a given foil). This suggests that there may be some heterogeneity in phosphorus segregation, although all the thin foils were extracted within the same grain as shown if Fig. 1. This possible segregation heterogeneity may also partly explain why slightly different values are obtained among the different techniques used, as those techniques do not probe exactly the same volume of material.

The second hypothesis is related to the quantification models used in the different methods. Quite sophisticated models are used, especially for AR-XPS and WDS. Those models involve several constants as input parameters that are taken from literature. For AR-XPS for example, the needed parameters are the photo-electric cross-sections, the inelastic mean free paths, the transport mean free paths and the asymmetric parameters. All of those parameters are subject to some uncertainty, which might affect the final quantification result. The same observation can be made for the WDS method were a lot of constants taken from literature are involved in the model implemented in the Stratagem software [30]. To a lesser extent, this is also true for the other methods, where, although the quantification models are not as

sophisticated, parameters taken from literature are also involved, like ACF in STEM-EDX for example. As the four methods used in this work are very different in nature, they rely on different quantification models and different input parameters, all of those parameters being subject to some uncertainty. This can contribute to the differences observed among the quantifications obtained from the four methods used in this work.

Table 1: Phosphorus and sulphur segregation quantification results in the sandwich specimen using AR-XPS, WDS, STEM-EDX and APT. The standard deviations shown are counting uncertainties.

Technique	**P concentration (atom/nm²)**	**S concentration (atom/nm²)**
AR-XPS	3.38 ± 0.11	3.05 ± 0.08
WDS	3.11 ± 0.03	3.94 ± 0.04
STEM-EDX	4.22 ± 0.01	3.86 ± 0.01
APT	4.6	-

Table 2: Phosphorus segregation quantification results obtained from STEM-EDX for the four thin foils analysed with the associated counting uncertainties.

Thin foil	Number of acquisitions	$S_P \pm \Delta S_P$
#1	7	3.86 ± 0.02
#2	9	3.97 ± 0.02
#3	7	4.96 ± 0.02
#4	6	4.12 ± 0.02
Total	29	4.22 ± 0.01

4 Conclusions

In this work, quantification of phosphorus and sulfur interface segregation in a Fe-P-Fe sandwich sample was conducted using different analytical techniques. Attention was paid to express the quantifications of the different methods in the same manner, i.e. surface/interface concentration in atom/nm², so as to allow direct comparison between them. Surface techniques, XPS and WDS, and bulk techniques, STEM-EDX and APT, were used. All measurements were performed within the same grain surface of the specimen, as close as possible to each other, to keep possible specimen related variations to a minimum. Despite the more complex structure of the Fe-P-Fe sample than a real grain boundary (because of the native oxide layer), the sandwich structure allowed for measurements by different techniques at different stages of the sample fabrication. The results obtained from the different techniques agree within approximately 0.5 to 0.7 atom/nm², which is reasonable considering the techniques used are very different in nature.

5 Acknowledgement

Special thanks to G. Espinasse and S. Violier for the WDS measurements.

6 Funding

This research was mainly funded by EDF (Electricité de France) with the support of ANRT (Association Nationale de la Recherche et de la Technologie).

7 References

[1] P. Lejcek, *Grain boundary segregation in metals*. Berlin: Springer-Verlag, 2010.
[2] C. A. English, S. R. Ortner, G. Gage, W. L. Server, and S. T. Rosinski, "Review of Phosphorus Segregation and Intergranular Embrittlement in Reactor Pressure Vessel Steels", doi: 10.1520/STP10531S.
[3] S.-G. Park, K.-H. Lee, M.-C. Kim, and B.-S. Lee, "Effects of boundary characteristics on resistance to temper embrittlement and segregation behavior of Ni–Cr–Mo low alloy steel," *Materials Science and Engineering: A*, vol. 561, pp. 277–284, Jan. 2013, doi: 10.1016/j.msea.2012.10.078.
[4] S. Raoul, B. Marini, and A. Pineau, "Effect of microstructure on the susceptibility of a 533 steel to temper embrittlement," *Journal of Nuclear Materials*, p. 7, 1998.
[5] S.-H. Song, Y. Zhao, Y. Cui, J. Sun, H. Si, and J.-Q. Li, "Effect of grain boundary character distribution and grain boundary phosphorus segregation on the brittleness of an interstitial-free steel," *Materials Letters*, vol. 182, pp. 328–331, Nov. 2016, doi: 10.1016/j.matlet.2016.07.023.
[6] D.-D. Shen, S.-H. Song, Z.-X. Yuan, and L.-Q. Weng, "Effect of solute grain boundary segregation and hardness on the ductile-to-brittle transition for a Cr–Mo low-alloy steel," *Materials Science and Engineering: A*, vol. 394, no. 1–2, pp. 53–59, Mar. 2005, doi: 10.1016/j.msea.2004.10.036.

[7] F. Christien and R. Le Gall, “Measuring surface and grain boundary segregation using wavelength dispersive X-ray spectroscopy,” *Surface Science*, vol. 602, no. 14, pp. 2463–2472, Jul. 2008, doi: 10.1016/j.susc.2008.05.017.
[8] P. Nowakowski, “Measuring grain boundary segregation using Wavelength Dispersive X-ray Spectroscopy: Further developments,” *Surface Science*, p. 11, 2011.
[9] A. Akhatova *et al.*, “Investigation of the dependence of phosphorus segregation on grain boundary structure in Fe-P-C alloy: cross comparison between Atom Probe Tomography and Auger Electron Spectroscopy,” *Applied Surface Science*, vol. 463, pp. 203–210, Jan. 2019, doi: 10.1016/j.apsusc.2018.08.085.
[10] L. Zhang, B. Radiguet, P. Todeschini, C. Domain, Y. Shen, and P. Pareige, “Investigation of solute segregation behavior using a correlative EBSD/TKD/APT methodology in a 16MND5 weld,” *Journal of Nuclear Materials*, vol. 523, pp. 434–443, 2019, doi: https://doi.org/10.1016/j.jnucmat.2019.06.002.
[11] V. J. Keast and D. B. Williams, “Grain boundary chemistry,” *Current Opinion in Solid State and Materials Science*, vol. 5, no. 1, pp. 23–30, Jan. 2001, doi: 10.1016/S1359-0286(00)00029-2.
[12] V. J. Keast and D. B. Williams, “Quantification of boundary segregation in the analytical electron microscope,” *J Microsc*, vol. 199, no. 1, pp. 45–55, Jul. 2000, doi: 10.1046/j.1365-2818.2000.00694.x.
[13] T. Walther, A. Rečnik, and N. Daneu, “A Novel Method of Analytical Transmission Electron Microscopy for Measuring Highly Accurately Segregation to Special Grain Boundaries or Planar Interfaces,” *Microchimica Acta*, vol. 155, no. 1–2, pp. 313–318, Sep. 2006, doi: 10.1007/s00604-006-0562-5.
[14] D. B. Williams, M. Watanabe, A. J. Papworth, and J. C. Li, “Quantitative characterization of the composition, thickness and orientation of thin films in the analytical electron microscope,” *Thin Solid Films*, vol. 424, no. 1, pp. 50–55, Jan. 2003, doi: 10.1016/S0040-6090(02)00906-9.
[15] J. A. S. Ikeda, Y.-M. Chiang, A. J. Garratt-Reed, and J. B. V. Sande, “Space Charge Segregation at Grain Boundaries in Titanium Dioxide: II, Model Experiments,” *Journal of the American Ceramic Society*, vol. 76, no. 10, pp. 2447–2459, 1993, doi: 10.1111/j.1151-2916.1993.tb03965.x.
[16] T. Hu, S. Yang, N. Zhou, Y. Zhang, and J. Luo, “Role of disordered bipolar complexions on the sulfur embrittlement of nickel general grain boundaries,” *Nature Communications*, vol. 9, no. 1, p. 2764, Jul. 2018, doi: 10.1038/s41467-018-05070-2.
[17] P. Doig and P. E. J. Flewitt, “STEM-EDS X-ray microanalysis of grain boundary segregations: The influence of electron probe size and grain boundary orientation,” *Micron and Microscopica Acta*, vol. 14, no. 3, pp. 225–231, Jan. 1983, doi: 10.1016/0047-7206(83)90053-5.
[18] M. Allart, F. Christien, R. Le Gall, P. Nowakowski, and C. R. M. Grovenor, “A multi-technique investigation of sulfur grain boundary segregation in nickel,” *Scripta Materialia*, vol. 68, no. 10, pp. 793–796, May 2013, doi: 10.1016/j.scriptamat.2013.01.028.
[19] P. Doig, P. E. J. Flewitt, and R. K. Wild, “A comparison of X-ray (STEM) and Auger electron spectroscopy for the microanalysis of grain boundary segregation,” *Philosophical Magazine A*, vol. 37, no. 6, pp. 759–768, Jun. 1978, doi: 10.1080/01418617808239206.
[20] A. Partridge and G. J. Tatlock, “A comparison of Auger and STEM-EDS quantification routines used in an investigation of intergranular segregation in long-term aged nimonic PE16,” *Surface and Interface Analysis*, vol. 18, no. 10, pp. 713–723, Oct. 1992, doi: 10.1002/sia.740181005.
[21] S. J. Wu, R. G. Ding, and J. F. Knott, “Statistical analysis of phosphorus segregation on intergranular fracture facets in pressure vessel steels,” *Materials Science and Technology*, vol. 23, no. 11, pp. 1262–1268, 2007, doi: 10.1179/174328407X154248.
[22] I. A. Vatter and J. M. Titchmarsh, “Comparison of FEG-STEM and AES Measurements of Equilibrium Segregation of Phosphorus in 9% Cr Ferritic Steels,” *SURFACE AND INTERFACE ANALYSIS*, vol. 25, p. 17, 1997.

[23] C.-Y. Hsu, J. Stodolna, P. Todeschini, F. Delabrouille, B. Radiguet, and F. Christien, “Accurate quantification of phosphorus intergranular segregation in iron by STEM-EDX,” *Micron*, vol. 153, p. 103175, Feb. 2022, doi: 10.1016/j.micron.2021.103175.
[24] J. Weidow and H.-O. Andrén, “Grain and phase boundary segregation in WC–Co with small V, Cr or Mn additions,” *Acta Materialia*, vol. 58, no. 11, pp. 3888–3894, Jun. 2010, doi: 10.1016/j.actamat.2010.03.038.
[25] I. A. Vatter and J. M. Titchmarsh, “Measurement of grain-boundary segregation by STEM-EDX analysis,” *Ultramicroscopy*, vol. 28, no. 1, pp. 236–239, 1989, doi: https://doi.org/10.1016/0304-3991(89)90301-X.
[26] P. Doig, D. Lonsdale, and P. E. J. Flewitt, “Segregation of embrittling elements to prior austenite grain boundaries in 2·25Cr–1 Mo steel,” *Metal Science*, vol. 16, no. 7, pp. 335–344, Jul. 1982, doi: 10.1179/030634582790427488.
[27] R. G. Faulkner, S.-H. Song, and P. E. J. Flewitt, “Combined quenching and tempering induced phosphorus segregation to grain boundaries in 2-25Cr-1 Mo steel,” *Materials Science and Technology*, vol. 12, pp. 818–822, 1996, doi: 10.1179/mst.1996.12.10.818.
[28] S. Tougaard, “Universality Classes of Inelastic Electron Scattering Cross-sections,” *Surface and Interface Analysis*, vol. 25, no. 3, pp. 137–154, Mar. 1997, doi: 10.1002/(SICI)1096-9918(199703)25:3<137::AID-SIA230>3.0.CO;2-L.
[29] S. Tanuma, C. J. Powell, and D. R. Penn, “Calculations of electron inelastic mean free paths (IMFPS). IV. Evaluation of calculated IMFPs and of the predictive IMFP formula TPP-2 for electron energies between 50 and 2000 eV,” *Surface and Interface Analysis*, vol. 20, no. 1, pp. 77–89, Jan. 1993, doi: 10.1002/sia.740200112.
[30] J.-L. Pouchou, “X-Ray Microanalysis of Stratified Specimens,” *Analytica Chimica Acta*, vol. 283, pp. 81–97, 1993, doi: 10.1016/0003-2670(93)85212-3.
[31] S. Suzuki, K. Yanagihara, and K. Hirokawa, “XPS study of oxides formed on the surface of high-purity iron exposed to air,” *Surface and Interface Analysis*, vol. 30, no. 1, pp. 372–376, 2000, doi: 10.1002/1096-9918(200008)30:1<372::AID-SIA721>3.0.CO;2-R.
[32] G. Parkinson, “Iron Oxide Surfaces,” *Surface Science Reports*, 2016, doi: 10.1016/j.surfrep.2016.02.001.
[33] G. Cliff and G. W. Lorimer, “The quantitative analysis of thin specimens,” *Journal of Microscopy*, vol. 103, no. 2, pp. 203–207, Mar. 1975, doi: 10.1111/j.1365-2818.1975.tb03895.x.
[34] P. J. Sheridan, “Determination of experimental and theoretical kASi factors for a 200-kV analytical electron microscope,” *Journal of Electron Microscopy Technique*, vol. 11, no. 1, pp. 41–61, Jan. 1989, doi: 10.1002/jemt.1060110107.
[35] R. E. Connelly, C. S. Fadley, and P. J. Orders, “Quantitative analysis of a submonolayer adsorption system by angle resolved XPS: c(2×2)S on Ni(001),” *Journal of Vacuum Science & Technology A*, vol. 2, no. 3, pp. 1333–1338, Jul. 1984, doi: 10.1116/1.572404.
[36] A. Jablonski, “Universal quantification of elastic scattering effects in AES and XPS,” *Surface Science*, vol. 364, no. 3, pp. 380–395, Sep. 1996, doi: 10.1016/0039-6028(96)80112-9.
[37] A. Jablonski and I. S. Tilinin, “Towards a universal description of elastic scattering effects in X-ray photoelectron spectroscopy,” *Journal of Electron Spectroscopy and Related Phenomena*, vol. 74, no. 3, pp. 207–229, Nov. 1995, doi: 10.1016/0368-2048(95)02368-2.
[38] A. Jablonski, F. Salvat, and C. J. Powell, “Comparison of Electron Elastic-Scattering Cross Sections Calculated from Two Commonly Used Atomic Potentials,” *Journal of Physical and Chemical Reference Data*, vol. 33, no. 2, pp. 409–451, Jun. 2004, doi: 10.1063/1.1595653.
[39] S. Chandrasekhar, *Radiative Transfer Clarendon Press*. Oxford, 1950.

8 Appendix 1: Demonstration of equation *(1)*

The surface concentrations S_f in atom/nm^2 of impurities (phosphorus and sulfur) segregated in a monolayer at the surface of pure iron sample were estimated from AR-XPS measurements using an overlayer/substrate repartition model. Based on the work of Fadley [35], it can be shown that choosing the appropriate photoelectron peak especially for the substrate (Fe_{3p} instead of the more intense Fe_{2p} one) allows assumptions leading to a linear expression between the ratio I_f / I_s and the inverse of the cosine of the photoelectron emission angle α relative to the normal of the sample where I_f and I_s are respectively the intensities of photoelectron peaks from the segregated monolayer (P_{2p} or S_{2p}) and the substrate (Fe_{3p}).

The intensity I_s of substrate photoelectron peak can be described by the following expression:

$$I_s = \Delta\Omega T\left(E_s\right) DFA_0 \left(\frac{d\sigma_x}{d\Omega}\right)_s \times N_s \lambda_{in}^s \left(E_s\right) \exp\left(\frac{-d}{\lambda_{in}^f \left(E_s\right)\cos\alpha}\right) \qquad (5)$$

Where F is the X-ray flux, D is the detector efficiency, $\Delta\Omega$ is the acceptance solid angle of the analyser, A_0 the analysis area for photoemission normal to the surface, $T(E_s)$ is the analyser transmission function at the kinetic energy E_s of photoelectrons coming from the substrate, N_s is the number of substrate atoms in unit volume, λ_{in}^s and λ_{in}^f are respectively the inelastic mean free path of electrons coming from the substrate with kinetic energy E_s and travelling through the substrate and the overlayer, $\left(\frac{d\sigma_x}{d\Omega}\right)_s$ is the differential photoelectric cross-section of the core level x considered for the intensity photoelectron peak and *d* is the thickness of the submonolayer film made up of segregated species. Taking the anisotropy of photoemission into consideration, this cross section has the following form:

$$\left(\frac{d\sigma_x}{d\Omega}\right)_s = \sigma_x^{(s)} W\left(\beta^{(s)},\psi\right) = \sigma_x^{(s)} \frac{1}{4\pi}\left[1-\frac{\beta^{(s)}}{4}\left(3\cos^2\psi-1\right)\right] \qquad (6)$$

Where $\sigma_x^{(s)}$ is the total photoelectric cross-section, $\beta^{(s)}$ is the asymmetry parameter and ψ is the angle between the incident X-ray radiation and the photoemission.

As described in the work of Fadley [35], in the case of quantitative analysis of submonolayer system, the signal from the substrate choosing a core level producing photoelectron at high kinetic energy (Fe_{3p} at 1432 eV in this work) is nearly not affected by inelastic attenuation in the overlayer for $\alpha \leq 70^0$ which makes it possible to simplify the equation (5) into the following expression:

$$I_s = \Delta\Omega T\left(E_s\right) DFA_0 \left(\frac{d\sigma_x}{d\Omega}\right)_s \times N_s \lambda_{in}^s\left(E_s\right) \qquad (7)$$

However, the signal from the substrate can be influenced by elastic scattering. In order to take account for elastic scattering effects, Jablonski proposed [36] to modify the differential photoelectric cross-section using two correction factors Q_x and β_{eff} leading to the equations (*8*) and (*9*):

$$I_s = \Delta\Omega T\left(E_s\right) DFA_0 \left(\frac{d\sigma_x}{d\Omega}\right)_s^{\text{mod}} \times N_s \lambda_{in}^s\left(E_s\right) \qquad (8)$$

$$\left(\frac{d\sigma_x}{d\Omega}\right)_s^{\text{mod}} = \sigma_x^{(s)} Q_x^{(s)} W\left(\beta_{eff}^{(s)},\psi\right) = \sigma_x^{(s)} Q_x^{(s)} \frac{1}{4\pi}\left[1-\frac{\beta_{eff}^{(s)}}{4}\left(3\cos^2\psi-1\right)\right] \qquad (9)$$

The two correction factors are defined by the single scattering albedo ω [37] which as shown in the equation *(10)* measures the relative strengths of elastic and inelastic scattering using the inelastic mean free path λ_{in} and the transport mean free path λ_{tr} related to the elastic scattering cross section [38].

$$\omega = \frac{\lambda_{in}}{\lambda_{tr}+\lambda_{in}} \qquad (10)$$

Using the H function of Chandrasekar [39] the two factors are described by the following expressions:

$$Q_x = (1-\omega)^{1/2} H(\cos\alpha, \omega) \qquad (11)$$

$$\beta_{eff} = (1-\omega)\frac{\beta}{Q_x} \qquad (12)$$

In the same way, the intensity I_f of overlayer photoelectron peak can be described by the following expression:

$$I_f = \Delta\Omega T(E_f) DFA_0 \sigma_x^{(f)} Q_x^{(f)} W(\beta_{eff}^{(f)}, \psi) N_f \lambda_{in}^f(E_f) \left[1 - \exp\left(\frac{-d}{Q_x^{(f)} \lambda_{in}^f(E_f)\cos\alpha}\right)\right] \qquad (13)$$

Depending on the nature of the species, phosphorus or sulfur, the photo-ionized core level x corresponds either to P_{2p} or S_{2p}. It is worth noting that the elastic scattering factor Q_x appears also in the exponential term. The product of Q_x with the inelastic mean free path λ_{in}^f gives rise to an effective attenuation length. At the respective kinetic energies 1358 eV and 1325 eV for P_{2p} and S_{2p} peaks, this effective attenuation length is more than one order of magnitude larger than *d*, which allows to simplify equation *(13)* according to the following expression:

$$I_f \approx \Delta\Omega T(E_f) DFA_0 \sigma_x^{(f)} W(\beta_{eff}^{(f)}, \psi) \frac{N_f d}{\cos\alpha} \qquad (14)$$

This assumption allows to access to the surface concentration S_f in atom/nm^2 of the considered impurities as shown in equation *(15)*.

$$I_f \approx \Delta\Omega T(E_f) DFA_0 \sigma_x^{(f)} W(\beta_{eff}^{(f)}, \psi) \frac{S_f}{\cos\alpha} \qquad (15)$$

According to equations *(8)*, (*9*) and *(15)*, we deduce a simple expression for the ratio I_f / I_s :

$$\frac{I_f}{I_s}=\frac{T\left(E_f\right)}{T\left(E_s\right)}\frac{\sigma_x^{(f)}W\left(\beta_{eff}^{(f)},\psi\right)}{\sigma_x^{(s)}W\left(\beta_{eff}^{(s)},\psi\right)}\frac{S_f}{Q_x^{(s)}N_s\lambda_{in}^s\left(E_s\right)\cos\alpha} \qquad (16)$$

Moreover the kinetic energies for overlayer photoelectron peak (1358 eV and 1325 eV for P_{2p} and S_{2p}) and substrate photoelectron peak (1432 eV for Fe_{3p}) are close and in a region were the variation of transmission function is weak ($T\left(E_f\right)\approx T\left(E_s\right)$) leading to the following final expression:

$$\frac{I_f}{I_s}\frac{\sigma_x^{(s)}W\left(\beta_{eff}^{(s)},\psi\right)}{\sigma_x^{(f)}W\left(\beta_{eff}^{(f)},\psi\right)}Q_x^{(s)}N_s\lambda_{in}^s\left(E_s\right)=\frac{S_f}{\cos\alpha} \qquad (17)$$

Two linear expressions can then be formulated in order to determine from intensities of P_{2p}, S_{2p} and Fe_{2p} the surface concentrations of phosphorus and sulfur segregated impurities S_P and S_S :

$$\frac{I_{P2p}}{I_{Fe3p}}\frac{\sigma_{Fe3p}W\left(\beta_{eff}^{Fe3p},\psi\right)}{\sigma_{P2p}W\left(\beta_{eff}^{P2p},\psi\right)}Q_{Fe3p}^{(Fe)}N_{Fe}\lambda_{in}^{Fe}\left(E_{Fe3p}\right)=\frac{S_P}{\cos\alpha} \qquad (18)$$

$$\frac{I_{S2p}}{I_{Fe3p}}\frac{\sigma_{Fe3p}W\left(\beta_{eff}^{Fe3p},\psi\right)}{\sigma_{S2p}W\left(\beta_{eff}^{S2p},\psi\right)}Q_{Fe3p}^{(Fe)}N_{Fe}\lambda_{in}^{Fe}\left(E_{Fe3p}\right)=\frac{S_S}{\cos\alpha} \qquad (19)$$

To determine $W\left(\beta_{eff}^{Fe3p},\psi\right)$, $W\left(\beta_{eff}^{P2p},\psi\right)$, $W\left(\beta_{eff}^{S2p},\psi\right)$ and $Q_{Fe3p}^{(Fe)}$, respective values of 1.455, 1.09 and 1.151 were chosen for the asymmetric parameters β_{Fe3p}, β_{P2p} and β_{S2p} as well as transport mean path values taken from the software for Simulation of Spectra for Surface analysis SESSA using NIST electron scattering cross section database. The values of $W\left(\beta_{eff}^{Fe3p},\psi\right)$, $W\left(\beta_{eff}^{P2p},\psi\right)$, $W\left(\beta_{eff}^{S2p},\psi\right)$ and $Q_{Fe3p}^{(Fe)}$ are reported in function of the angles α and ψ in table A1.

Table A1: calculated values of photoemission cross section anisotropy function $W\left(\beta_{eff}^{Fe3p},\psi\right)$, $W\left(\beta_{eff}^{P2p},\psi\right)$, $W\left(\beta_{eff}^{S2p},\psi\right)$ and elastic scattering factor in the Fe substrate $Q_{Fe3p}^{(Fe)}$ for different angles α and ψ configurations.

α (°)	ψ (°)	$W\left(\beta_{eff}^{Fe3p},\psi\right)$	$W\left(\beta_{eff}^{P2p},\psi\right)$	$W\left(\beta_{eff}^{S2p},\psi\right)$	$Q_{Fe3p}^{(Fe)}$
25	44.5	0.865	0.901	0.893	0.919
35	52.3	0.968	0.976	0.975	0.914
45	60.5	1.072	1.053	1.057	0.907
55	69.1	1.163	1.121	1.129	0.897
65	77.8	1.232	1.173	1.184	0.882
75	86.6	1.271	1.202	1.215	0.862